CrossMark

Application of MAVEN Accelerometer and Attitude Control Data to Mars Atmospheric Characterization

**Richard W. Zurek · Robert H. Tolson · Darren Baird ·
Mark Z. Johnson · Stephen W. Bougher**

Abstract The structure of the upper atmosphere of Mars (above ∼100 km) has been probed in situ mainly using spacecraft accelerometers during the aerobraking phases of 3 Mars orbiters. In a similar manner, the Mars Atmosphere and Volatile Evolution (MAVEN) Accelerometer Experiment (ACC) will also use atmospheric drag accelerations sensed by inertial measurement units (IMU) onboard the spacecraft to recover atmospheric density along the orbiter path. These densities are used to estimate hydrostatic 'vertical' density and temperature profiles, along track and altitudinal density waves, and latitudinal and longitudinal density variations. The IMU accelerometer signal-to-noise should permit profile reconstructions from spacecraft periapsis, nominally at 150 km altitude, to ∼ 170 km, an altitude range nominally spanning densities of 0.05–0.15 kg/km^3. However, in situ measurements over a much greater altitude range, down to ∼125 km (reaching densities of ∼2–3.5 kg/km^3), can be made during each of five week-long "Deep Dip" (DD) campaigns, and these are the prime focus of the Accelerometer Experiment. Judicious choice of the timing of these Deep-Dip campaigns during the MAVEN periapsis progression through local time, latitude and longitude in both hemispheres and in different seasons will add significantly to the existing data base of lower thermospheric densities. Other IMU and attitude control data may be used to estimate torques in order to improve the atmospheric density analysis, especially

R.W. Zurek (✉)
Jet Propulsion Laboratory, California Institute of Technology, Mail Stop 321-690, 4800 Oak Grove
Drive, Pasadena, CA 91109, USA
e-mail: richard.w.zurek@jpl.nasa.gov

R.H. Tolson
National Institute of Aerospace, 100 Exploration Way, Hampton, VA 23666, USA

D. Baird
NASA Johnson Space Flight Center, 2101 NASA Parkway, Houston, TX 77058, USA

M.Z. Johnson
Lockheed Martin Space Systems Corporation, Denver, CO, USA

S.W. Bougher
University of Michigan, 2455 Hayward Ave., Ann Arbor, MI 48109-2143, USA

in the higher altitudes of the nominal science orbit, and, more challengingly, to estimate cross-track winds during the Deep-Dips.

1 Introduction

The Mars Atmosphere and Volatile Evolution (MAVEN) mission seeks to characterize the current structure and processes of the Mars upper atmosphere and its interactions with the solar wind in order to evaluate and extrapolate in time those processes contributing to the escape of atmospheric gases, particularly volatiles, over the long history of Mars (Jakosky et al. 2014, this issue). In situ measurements of atmospheric density in the Mars thermosphere over a range of local time and planetary latitude-longitude during the one-Earth year of the MAVEN prime mission are a critical part of that characterization.

Spacecraft (s/c) drag is a traditional method for determining the thermospheric density of a planetary atmosphere. The introduction of precise, onboard accelerometers significantly improved the spatial and temporal resolution and accuracy of density recovery. These precision devices also enabled reliable aero-maneuvering in the thin outer reaches of planetary atmospheres. For Mars this meant the development of aerobraking as a practical procedure to get orbiters at Mars into the desired science orbits with a minimum use of fuel, saving on launch mass and mission costs.

During an aerobraking phase, the orbiter periapsis is lowered using very small propulsive maneuvers into the denser regions of the atmosphere where increased atmospheric drag reduces the spacecraft momentum, thereby reducing the altitude of apoapsis. The spacecraft team aims periapsis for an altitude where the density is not great enough that atmospheric friction will overheat the spacecraft, but also where the density is not so low that the atmospheric drag is ineffective. The difficulty, of course, is that the density at a given altitude high in a planetary atmosphere changes with time and place. Typically, the orbit-to-orbit change in density at a given altitude is ∼30 %, but on occasion it can be much greater, especially when there is increased dust storm activity in the lower atmosphere. Precise density estimates, derived from tracking the satellite and/or from the onboard accelerometers, are critical to ensuring that the spacecraft periapsis is maintained in a safe, but effective corridor.

The desired margin of safety typically means that the change on any on orbit is small, but repeated drag passes enable major changes to the orbit without requiring a large mass of onboard propellant. Three missions—Mars Global Surveyor (MGS) launched in 1996, Mars Odyssey (ODY) launched in 2001 and Mars Reconnaissance Orbiter (MRO) launched in 2005—have successfully aerobraked at Mars during hundreds of orbits spanning periods from a few to several months. In turn, these extended periods of aerobraking have permitted atmospheric densities in the lower Mars thermosphere to be derived for significant, but incomplete, portions of various Mars years and local times of day.

Such measurements at Mars have identified a rapid thermospheric response to a regional dust storm (Keating et al. 1998), a high-altitude polar warming (Keating et al. 2003; Bougher et al. 2006), gravity waves (Fritts et al. 2006), and tides (Forbes et al. 2002). They have also provided significant tests of Mars atmospheric circulation models and pointed to specific needs in the model physical parameterizations (see Bougher et al. 2006, 2008, and references therein). MAVEN will continue this tradition through the Accelerometer (ACC) Experiment and an associated Atmospheric Analysis Group (AAG) which will intercompare ACC density estimates with results from other MAVEN experiments and with atmospheric models.

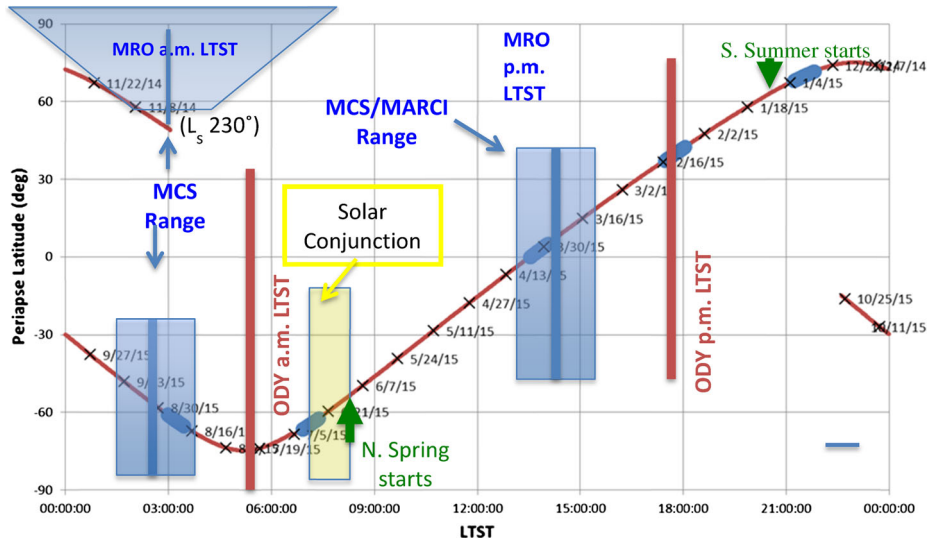|	Deep Dip #	Start date	Center latitude	Center LTST	L_s
Table 1 Deep Dip campaign attributes	1	12/28/14	70N	21.5	261
	2	2/9/15	40N	17.5	288
Note: Dates and coordinates are approximate and will be finalized after entry into the final science orbit and check-out of the science payload	3	3/28/15	2N	13.5	316
	4	6/22/15	62S	7.0	2
	5	8/17/15	61S	3.5	28

Fig. 1 The trace (*red curve*) of the MAVEN periapsis in latitude and local true solar time during the one year of the MAVEN primary science mission. Time is marked along the trace in 2-week increments. The *blue ovals* indicate the ~10 day long Deep Dip campaigns, although the indicated timing of these may be adjusted once MAVEN is in its science orbit. Local times that can be viewed by MRO instruments (*blue*) and by ODY (*red*) are schematically represented

MAVEN does not aerobrake in the sense that its prime science orbit is established only by propulsive maneuvers (Jakosky et al. 2014, this issue). However, MAVEN will execute five "Deep Dip" (DD) campaigns that are effectively aerobraking mini-phases, too short to significantly perturb the orbit, but permitting in situ measurements lower in the thermosphere and closer to the homopause. Table 1 shows the present expectations for the timing, latitude and local true solar time (LTST) of the DD. Figure 1 puts these DD in the context of the MAVEN periapsis evolution during the one (Earth) year of the primary science mission. Also shown are the local times that instruments on the Mars Reconnaissance Orbiter (MRO Mars Climate Sounder and Mars Color Imager) and Mars Odyssey (ODY THEMIS) spacecraft may be observing the lower atmosphere; these are prime times for synergistic observations.

The DD campaigns occur near local solar times (LST) of midnight, dawn, noon, sunset polar night. The first DD occurs just before $L_s = 270°$, the southern summer/northern winter solstice. [L_s, the areocentric longitude of the Sun as seen at Mars is used to indicate the seasonal date (i.e., time of the Mars year). $L_s = 0° = 360°$ identifies the vernal (northern
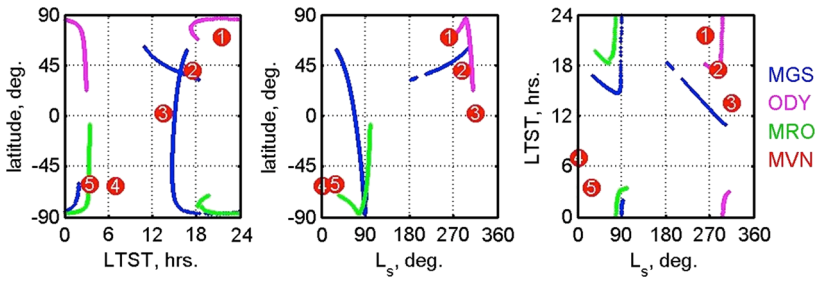
Fig. 2 Latitudinal, seasonal, and diurnal periapsis coverage from MAVEN during the Deep Dips (*red dots*, numbered as in Table 1) and (*curves*) from three aerobraking missions (MGS, ODY, MRO). Aerobraking periapsis altitudes from these missions ranged from 95 to 120 km. Meaningful atmospheric densities were recovered from periapsis altitude up to 170 km on each mission. MAVEN data will fill key gaps and provide assessment of interannual and solar cycle variability

spring) equinox.] This is a seasonal period when vast dust storms—a few encircling the planet—have occurred in some, but not all Mars years. The last DD occurs near $L_s = 30°$, early in northern spring, entering a period when the lower Mars atmosphere has tended to be remarkably repeatable from (Mars) year to year. Each campaign will last 7–10 days during which periapsis is lowered to an altitude ∼125 km where the density is nominally between 2 and 3.5 kg/km^3.

Communications between Earth and the MAVEN spacecraft are uncertain and therefore restricted during the Solar Conjunction period, the extent of which is conservatively represented in Fig. 1. A Deep-Dip campaign would not be conducted without daily contact with the DSN. The schedule for this (and all other DD) campaign will be adjusted once MAVEN's science orbit is precisely known. For now, Fig. 1 is representative of the regimes to be explored by DD.

Figure 2 shows the latitudinal-seasonal-diurnal coverage of the MAVEN DD campaigns against the historical coverage (Tolson et al. 2007) acquired during MGS, ODY and MRO aerobraking phases. The MAVEN Deep Dip campaigns are designed to complement the coverage from these prior missions by filling key gaps in the latitudinal, seasonal, diurnal coverage charts or by capturing interannual variability. The major unexplored regions remain the southern hemisphere spring and summer, either summer pole and morning hours in general. The aerobraking missions had orbit inclinations of around 93° and provided, during each periapsis pass, an opportunity to observe latitudinal density gradients and small-scale latitudinal wave structure, often interpreted as vertically propagating gravity waves. With an orbit inclination of 75°, MAVEN will provide, at high latitudes, the first opportunity to observe small-scale longitudinal variations.

2 The Spacecraft as Instrument: Accelerometers and Other Data Types

Reference will often be made to the s/c body coordinate system, orientation of the relative wind, cross winds, and other characteristics. This reference coordinate system is shown in Fig. 3. The s/c *z*-axis is along the center-line of the high-gain antenna, and the *x*-axis is parallel to the Articulated Pointing Platform (APP) boom which holds several instruments, including the Neutral Gas Ion Mapping Spectrometer (NGIMS, Mahaffy et al. 2014, this issue), which also makes in situ density measurements and which must account for wall effects and atmospheric winds.

Fig. 3 Coordinate system and vehicle characteristics of interest to the ACC experiment, including effects of winds
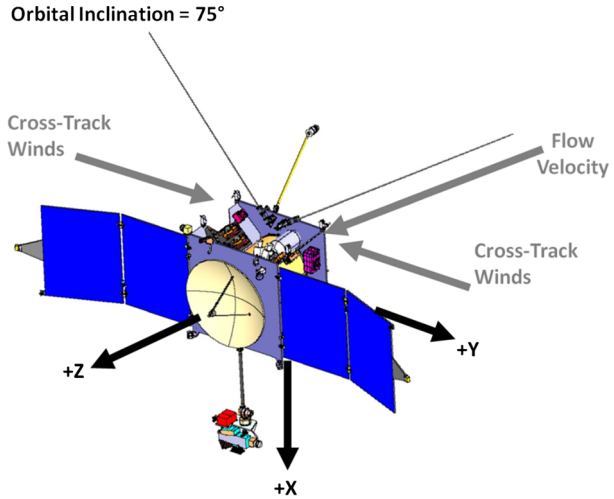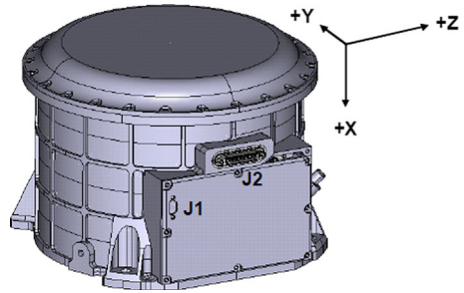

Fig. 4 Honeywell Miniature Inertial Measurement Unit (MIMU)

During the DD campaigns the s/c is oriented so that the solar arrays are trailing the s/c bus into the wind, thereby providing aerodynamic stability. The x-axis is nominally pointing towards the center of Mars, and the APP articulates slowly to track the relative wind. Due to geometric asymmetries, the s/c aerodynamic trim is a few degrees from the z-axis. Nevertheless, the dominant aerodynamic acceleration is along the s/c z-axis, and IMU accelerations along that axis are used to recover atmospheric density.

MIMU/Accelerometers　The primary ACC data sources are the accelerometers in the Honeywell block 3 Miniature Inertial Measurement Units (MIMU). An engineering drawing of this MIMU is shown in Fig. 4. Each MIMU contains three orthogonally mounted Honeywell QA-3000 accelerometers and three orthogonal GG 1320 ring laser gyroscopes. For redundancy, two MIMUs are mounted on the s/c as shown in Fig. 5. The principle acceleration used in the ACC analysis is the body z-axis that approximately aligns with the MIMU x-axis. Since the MIMU is not located at the center of mass of the s/c, sensed accelerations have to be corrected for angular acceleration and centrifugal terms produced by rigid body rotations of the spacecraft and by gravity gradients (Tolson et al. 2008). The effective acceleration sensing location for each accelerometer is known to 1 mm relative to the MIMU mounting location. The accelerometers continuously integrate acceleration to accumulate velocity change in each direction. Velocity counts are provided to the ACC team at 10 samples per second. The accelerometer bias and scale factor have a specified temperature sensitivity that is accommodated through in-flight calibration (discussed later).

**Fig. 5** MIMU and Star Tracker (ST) locations on the MAVEN spacecraft bus
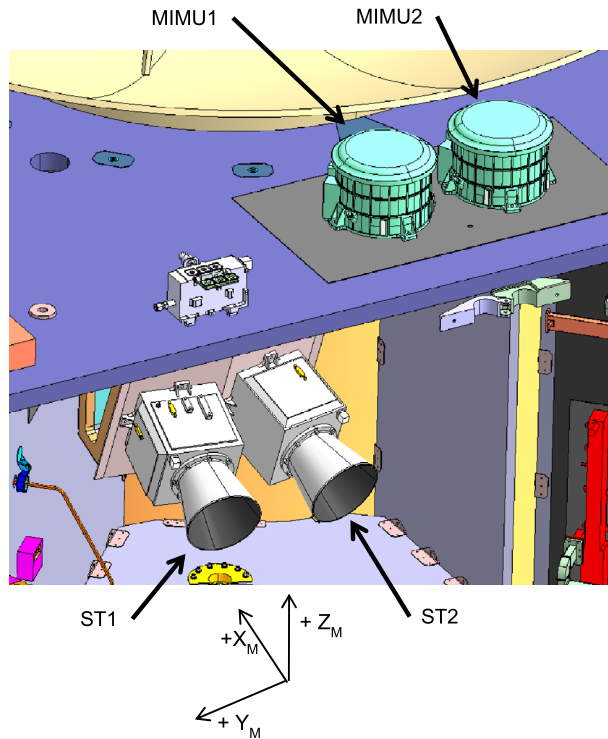
Accelerometer Sensitivity Each raw accelerometer count is equivalent to a change in velocity of 0.0753 mm/s. Actual acceleration is obtained by differencing two accumulated velocity measurements and dividing by the time difference. Hence temporal resolution can be traded against acceleration resolution. For a one-second average, this results in density recovery to about 0.02 kg/km^3 or about 1 % of the nominal DD maximum density.

In addition, the ACC team will analyze the accelerometer data together with other IMU and attitude control engineering data in an attempt to recover atmospheric density during the nominal (non-DD) science orbit where the density at periapsis is between 0.05 and 0.15 kg/km^3. This same combination of accelerometer and ancillary spacecraft data gathered during the DD campaigns may also allow calculation of zonal winds (see Sect. 6).

Accelerometer Bias There are a number of times during the mission, prior to the first Deep Dip campaign, that the accelerometer bias is determined. These calibrations are generally performed prior to any propulsive maneuver where the accelerometers are used to terminate the maneuver, for example MOI. The record of these bias estimations will be provided to the ACC team along with any relevant data that might explain changes in bias, e.g. MIMU or accelerometer temperatures. Gyro rate bias and scale factors are also determined during flight, and these and any relevant ancillary data will also be supplied to the ACC team as the calibrations are performed.

At the start of each DD periapsis pass, the accelerometer bias is automatically determined and telemetered as part of the ancillary data set available to the ACC team. This is done for both operational and scientific purposes. Further, during ACC team post-flight analysis, the bias is re-determined by fitting a line to the data before and after periapsis when the vehicle is little affected by atmospheric drag. An example from MRO aerobraking is shown in Fig. 6.

Fig. 6 The initially inferred acceleration on MRO orbit 101 is shown in the *lower panel* (the maximum acceleration is equivalent to $\rho = 76$ kg/km^3). The *upper panel* shows the data used to determine a time-linear bias model across the pass
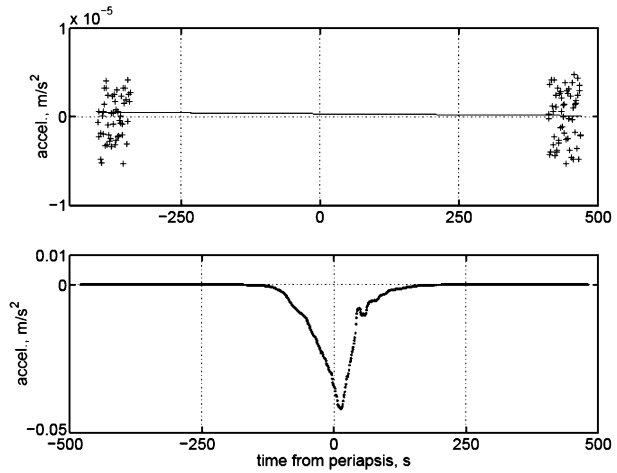
The lower panel shows the inferred acceleration throughout the entire atmospheric pass. The upper panel shows the data used to determine a time linear bias model across the pass. A small downward drift is noticed, but it is small compared to the data noise and has little statistical significance. For this orbit and most of the others, the automatic bias estimate eliminated essentially all of the bias. Nevertheless, bias removal is validated for each orbit.

3 Atmospheric Density Recovery

Basic Formula Atmospheric density (ρ) is determined by combining accelerations measured by the inertial measurement unit (MIMU), with s/c velocity determined by the Navigation team, and with an aerodynamic force coefficient database. The relevant expression is

$$\rho = \left(\frac{2M}{V^2 C_z A} \right) a_z \tag{1}$$

with spacecraft mass M, speed V relative to the atmosphere, aerodynamic force coefficient C_z along the z-axis of the s/c, reference area A, usually taken as the frontal area of the s/c when the wind is along the z-axis, and a_z, the acceleration of the s/c center of mass due to aerodynamic forces along the z-axis. The spacecraft mass M varies slightly during the mission due to propulsive maneuvers; estimates will be provided to ACC periodically during the mission. The inertial velocity comes from the Navigation team for each orbit and is transformed into velocity relative to the atmosphere by assuming the atmosphere is rigidly rotating with Mars (see below for an approach to estimating cross-track winds). This velocity is mapped into the spacecraft body frame using the vehicle attitude supplied by its attitude control system. Transforming the measured acceleration at the MIMU location to the center of mass using MIMU measured attitude angular rates then enables derivation of the acceleration of the center of mass.

Aerodynamic Force Coefficients The aerodynamic database is tabulated as a function of ρ and the orientation of the wind relative to the spacecraft. The orientation is defined by the x and y components of a unit vector along the relative wind, u_x and u_y respectively.
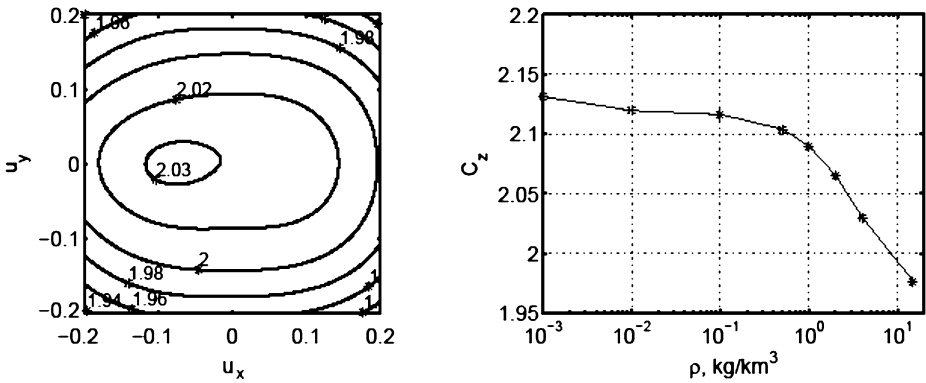
Fig. 7 Variation of the aerodynamic force coefficient along the spacecraft z-axis (C_z) with wind direction for $\rho = 4$ kg/km^3 (*left*) and variation with density ρ for flow along the z-axis (*right panel*)

For an atmospheric density of 4 kg/km^3, the left panel of Fig. 7 shows how the C_z force coefficient varies with the relative wind direction. Due to asymmetries about the spacecraft y–z plane, the maximum force occurs about 5° from $u_x = 0$. Spacecraft attitude during the DD is expected to remain within the range shown in the figure over which there is only a 3 % deviation in C_z from maximum to minimum. A somewhat larger change occurs at greater atmospheric densities.

The right panel of Fig. 7 demonstrates the variation with density of C_z at $u_x = u_y = 0$. At a density of 1 kg/km^3 the mean free path of a CO_2 molecule is about 160 m. Using 10 m as a characteristic length for the s/c leads to a Knudsen number of 16. As shown in the figure, this places the DD orbits at the beginning of the transition from free molecular to continuum flow. The Direct Simulation Monte Carlo program DAC provided by NASA was used to generate the aerodynamic database that will be used for MAVEN. The spacecraft geometry was provided by Lockheed-Martin and was an early version that does not include the recently added webbing to the ends of the solar arrays. The effects of this will be evaluated and factors will be updated. Since C_z is a function of density, Eq. (1) is solved recursively.

Error Sources Based on MRO, which flew the same IMU as does MAVEN, density is recoverable to about 0.1 kg/km^3 uncertainty. During Deep Dips, typical densities are ≈2.5 kg/km^3, yielding an error (noise) of ∼5 %. The aero database error is expected to be more like a bias, while the accelerometer noise is a more random component once bias is removed using the data (Fig. 6). With regard to the aero coefficient error, computational fluid dynamics (CFD) programs actually calculate pressure on the elements of the spacecraft. These pressures are integrated to get net forces and moments; these are then normalized into the non-dimensional aero coefficients by dividing by the dynamic pressure times a reference area A (see above) for forces and additionally a reference length L (typically the spacecraft maximum width) for moments. The CFD programs must assume a model for the gas-surface interaction between the atmosphere and the vehicle surface materials. This interaction is affected by many factors, including small-scale surface roughness, surface temperature and composition, gas composition and perhaps chemistry. However, spacecraft typically fly in the free molecular flow or transition region of the aero domain. In the free molecular flow regions this puts the drag coefficient near 2 in the thermosphere. Ignoring specular reflection, the effect of all the cited complicating factors add up to less than 10 % of this value.
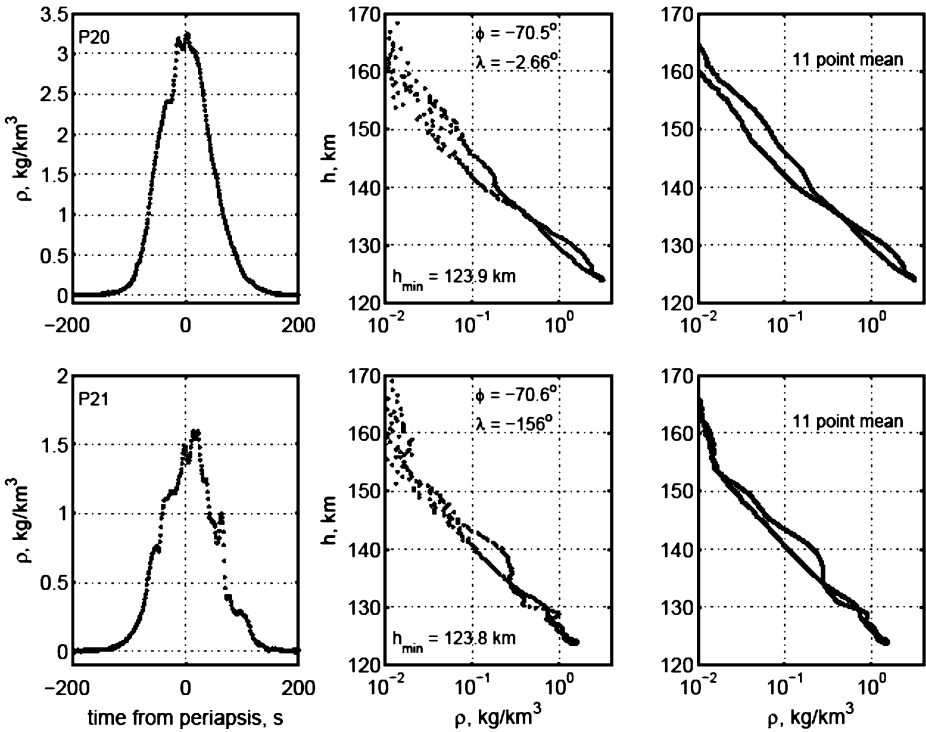
Fig. 8 MRO orbits 20 (*top*) and 21 (*bottom*) during its aerobraking walk-in phase. Densities were derived using 1-s samples (*left*, along track as a function of time from periapsis and *center*, as represented in a vertical profile) and using 11-s running mean (on *right*, as represented in a vertical profile). Periapsis altitude, latitude and longitude are indicated in the *center panels*

Moment coefficients vary more widely as they depend strongly on center of mass location and spacecraft asymmetry.

During the Deep Dip campaigns, there is 24/7 tracking of the vehicle. The MAVEN Navigation team will make estimates of atmospheric properties by scaling an engineering model of the thermosphere. One output on the Orbit Propagation and Timing Geometry (OPTG) file is the equivalent total δV change due to atmospheric forces. For each orbit, this δV will be compared with the total δV measured by the accelerometers. This provides a check of the accelerometer scale factor. During the past 3 aerobraking missions (MRO, ODY, MGS), differences were typically less than 2 %, 1-σ. Comparisons will also be made with NGIMS, providing the first opportunity for a Mars mission to compare neutral mass spectrometric results and accelerometer data, with their differing sets of measurement uncertainties.

4 Deep Dip Atmospheric Environment

Prior missions have provided a considerable amount of data on the atmospheric environment MAVEN can expect (Tolson et al. 2007) at the nominal DD and science orbit altitudes (Tolson et al. 2008). During the MRO walk-in phase there were two orbits near the DD density range, and these two orbits are reviewed here as surrogates for the ACC experiment. Figure 8 shows the derived atmospheric density vs. time from periapsis and vs. altitude. An

11-s running mean density profile is also provided. The orbital period is about 35 h for both orbits. The latitudes (ϕ) of the two orbits are less than 0.2° apart, and the minimum altitudes are within 100 m, which is small compared to the density scale height of about 7 km. The ratio of maximum densities is 2, suggesting the existence of strong longitudinal waves that might be due to tides (Forbes et al. 2002), even at these high latitudes. Note from Fig. 2 that the first DD will be near the LTST, L_s and latitude of the ODY mission. A polar warming was detected (Keating et al. 2003) during that mission, so an alternate explanation might be an off-axis polar warming. However, there is no indication of a significant longitudinal difference in temperature as inferred from the density scale height. In any case, factor of two changes in orbit-to-orbit density at Mars are not uncommon. On orbit 21 there is also some indication on the inbound leg of a vertical wave with 50 % deviations from what might be considered the mean profile. Such a wave might be a vertically propagating gravity wave, as it is predicted to have maximum amplitudes near the winter polar jet, i.e. 50°–70° latitudes (Fritts et al. 2006).

Note that MRO started aerobraking around latitudes of 70° S in the southern hemisphere winter. The first DD will occur at about 70N as the northern hemisphere winter begins. So the MRO surrogate may not be an unrealistic atmosphere for MAVEN to encounter. Since the nominal science orbit density range is 0.05 to 0.15 kg/km³, the periapsis altitude before and after the first DD could be as low as 140 km. The MAVEN MIMU should provide data with the same or better quality than MRO. So as mentioned earlier, density at DD periapsis will be well determined and the 1-s averaging can be extended to about 140 km or $\rho = 0.1$ kg/km³. Since the spacecraft has a horizontal velocity of about 4 km/s, the 1-s averaging provides 4 km along-track density resolution. By averaging over 11 s, the along-track resolution becomes about 40 km, but the averaged density appears realistic up to nearly 160 km or $\rho \sim 0.02$ kg/km³.

5 Operational Procedures and Products: Atmospheric Densities and Temperatures

During DD campaigns the ACC team will process data from the previous day, either 5 or 6 orbits of data. Quick-look products will be available to the planning teams, especially during the step-down orbits into the Deep Dips. Data products include the three components of center of mass acceleration corrected for the nominal offset of the MIMU from the center of mass at 1-s averaging vs. UTC (Greenwich) time in seconds and derived density at 1-s averaging vs. UTC time. Temperatures can also be derived assuming hydrostatic balance and symmetry with height (i.e., that the density profile represents a true vertical profile). After an initial phase to validate software and procedures, these products will normally be available daily with a one-day lag. Diagnostic plots will be generated for each pass, including bias estimation analysis like Fig. 6, density vs. time, and density vs. altitude like Fig. 8, along-track gradients, short-wavelength along-track wave analyses, and reference altitude densities and density scale height.

Products for delivery to the PDS Atmospheric node include, for each DD orbit, a file of time, altitude, density, density scale height, density 1-σ error, scale height 1-σ error, 39-s average altitude, 39-s. averaged density, and 39-s 1-σ density error. The new data will be combined with prior orbits to investigate long-term trends and potential longitudinal waves. Standard products will be supplied to the MAVEN science server for consideration by other science teams. Significant interaction is expected with the NGIMS team comparing derived total density measurements, with thermospheric modelers, and with the flight team assessing the state of the atmosphere from a mission operations viewpoint.

6 MAVEN Thermospheric Zonal Wind Calculations and Predictions

As illustrated in Fig. 3, the yaw orientation of the spacecraft (about the x axis) is sensitive to disturbances caused by cross-track winds acting on the spacecraft, which can significantly change the spacecraft heading. As discussed below, it may be possible to calculate the average cross-track winds throughout each aerobraking pass using Euler's equations of motion.

Euler's Equations of Motion   For a rigid body, Euler's equations of motion relate the external torques acting on the spacecraft to the time rate of change of spacecraft angular momentum. Cross-track winds can be calculated once all other external torques and time rates of change of angular momentum are determined from rate gyro, reaction wheel, and thruster data. For a first approximation the motion of the APP, the arm affixed to the bus and extending in the $+x$ direction, is ignored during each pass due to the expected low inner and outer gimbal rates. Euler's equation for the single, rigid-body system is then:

$$I_{s/c}\dot{\overline{\omega}}_{s/c} + \overline{\omega}_{s/c} \times I_{s/c}\overline{\omega}_{s/c} + J\dot{\overline{\Omega}} + \overline{\omega}_{s/c} \times J\overline{\Omega} = \frac{1}{2}\rho V_{s/c}^2 AL\overline{C}_m, \tag{2}$$

where $I_{s/c}$ is the moment of inertia of the spacecraft, $\overline{\omega}_{s/c}$ represents the angular velocity of the spacecraft as measured by the rate gyros, J is the moment of inertia of the reaction wheels, and $\overline{\Omega}$ represents the angular velocity of the reaction wheels. $V_{s/c}$ is the spacecraft velocity taken from ephemeris data, A is the reference cross-sectional area, L is the reference cross-sectional length, $\overline{C}_m$ is the aerodynamic moment coefficient and ρ is determined from Eq. (1). The left hand side of Eq. (2) can be calculated from telemetered body rate and reaction wheel speed data. $\overline{C}_m$, like C_z above, depends on u_x and u_y and is the only term in Eq. (2) that significantly depends on cross-track winds. As the spacecraft heading changes due to the wind, the right hand side of Eq. (2) therefore requires solving for the spacecraft velocity relative to the winds. The flow velocity is a summation of the spacecraft velocity and the wind velocity:

$$\overline{V}_{flow} = \overline{V}_{s/c} + \overline{V}_{wind} = \overline{V}_{s/c} + \overline{\omega} \times \overline{r}_{s/c} + U_{cw}\overline{e}_h \tag{3}$$

where $\overline{\omega} \times \overline{r}_{s/c}$ is the rigid atmospheric rotation, U_{cw} is the cross-track wind velocity, and $\overline{e}_h$ is the orbit angular momentum unit vector, assumed to be constant.

The aerodynamic torques about the x and y axes are solved using Eqs. (4) and (5), where the moment coefficients about the spacecraft x and y axes (C_{m_x} and C_{m_y}, respectively) are dependent on the cross-track winds:

$$N_x = \frac{1}{2}\rho \overline{V}_{s/c}^2 ALC_{m_x} \tag{4}$$

$$N_y = \frac{1}{2}\rho \overline{V}_{s/c}^2 ALC_{m_y} \tag{5}$$

Like C_z, moment coefficients C_{m_x} and C_{m_y} corresponding to the inferred density at each point during the aeropass are derived using multi-dimensional interpolation over a range of atmospheric densities from free molecular flow to deep in the transition region and a range of wind components that correspond to the known atmospheric densities.
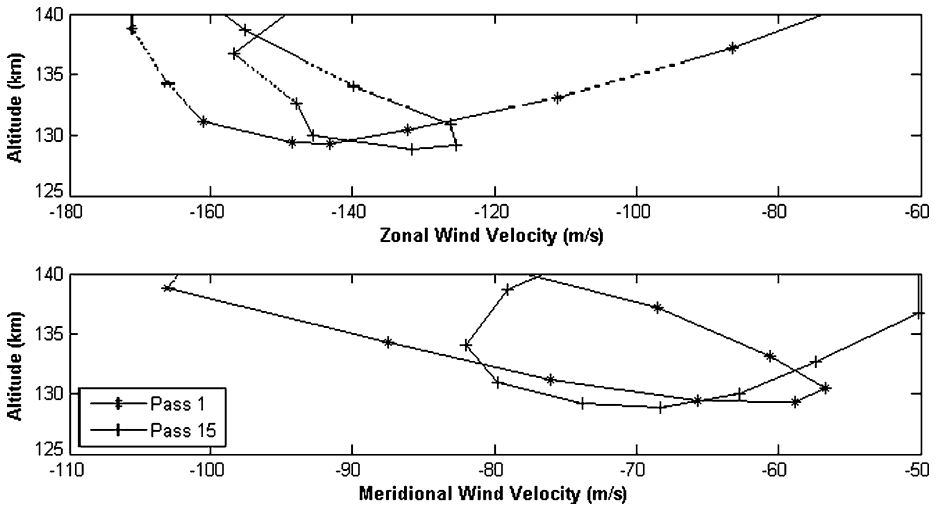
Fig. 9 MTGCM predicted wind fields for selected orbits during Deep-Dip 1 campaign (the periapsis passes [5–6 per day] are numbered from the start of the DD campaign)

Least-Squares Solution   A sensitivity analysis shows that a 1-cm change in the location of the spacecraft center of mass results in a 50 m/s change in recovered cross-track wind speed. To minimize the difference between the inertia-related and aerodynamic torques (left hand side and right hand side of Eq. (2), respectively), an iterative least-squares method will be used to solve for the average cross-track wind velocity of over the altitude range of each deep dip. Over a batch of orbits, the location of the spacecraft center of mass and the cross-track wind vector are varied. Upon completion of the iteration process, the cross-track winds that minimize the error of the least-squares equations, along with the associated uncertainties, are determined. The spacecraft center of mass can be held constant for each batch, and knowing the latitude at periapsis and the orbital inclination of 75°, the resulting cross track winds and uncertainties can be converted to zonal (east/west) and meridional (north/south) components. Based on similar calculations from the aerobraking phases of Mars Global Surveyor, 3-σ errors of ±10–50 m/s in the calculated cross-track winds are expected (Baird et al. 2007).

7 MTGCM Wind Predictions

Given the uncertainties in the wind calculations, it is useful to compare them to expected thermospheric wind values for the MAVEN mission and, specifically, the Deep Dips. Figures 9, 10 and 11 show the zonal and meridional thermospheric wind predicted by the Mars Thermospheric General Circulation Model (MTGCM; Bougher et al. 2008; Bougher 2012).

Figures 9–11 show MTGCM calculated winds (eastward and northward are positive in value) along selected spacecraft orbit tracks during Deep-Dip (DD) campaigns 1, 3, and 4, respectively, at altitudes from 125 km (near the expected periapsis altitude) to 140 km. The model uses a best estimate of F10.7 solar EUV flux set at 130×10^{-22} W/m²/Hz, and best estimates of dust conditions outside of dust storm season, based on the first year of Thermal Emission Spectrometer data (Smith 2004). The DD #1 campaign is scheduled near winter
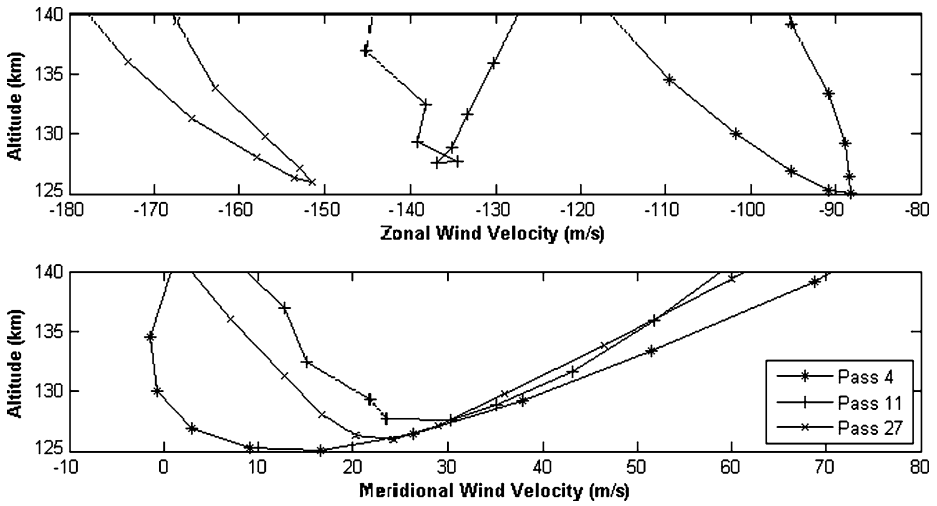
Fig. 10 MTGCM predicted wind fields for selected orbits during Deep-Dip 3 campaign
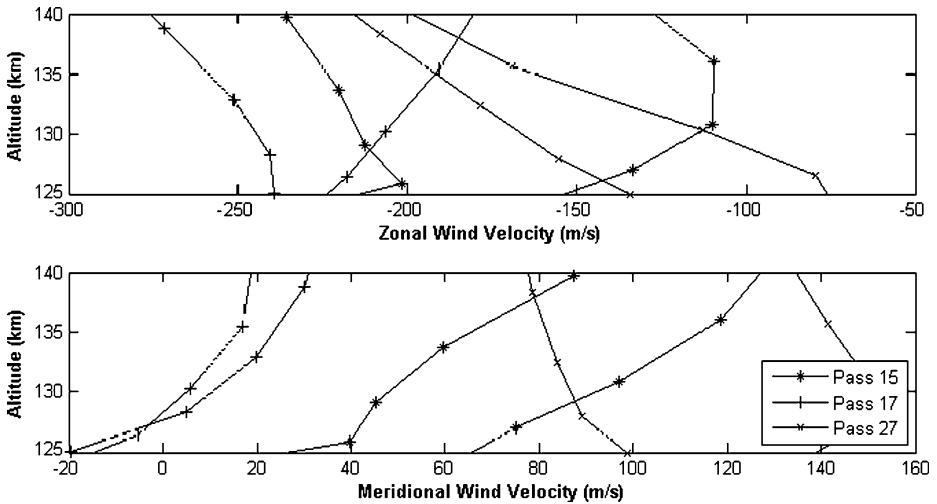

Fig. 11 MTGCM predicted wind fields for selected orbits during Deep-Dip 4 campaign

solstice ($L_s \sim 270°$); the DD #4 campaign is scheduled near spring equinox ($L_s = 0°$), while appropriately avoiding Solar Conjunction. DD #3 occurs near the end of the large dust storm season ($L_s = 330°$).

Because the wind derivation depends critically on precise knowledge of the spacecraft dynamical response and the strength of the winds, the wind-related data products are regarded as special products, which will be produced on a best efforts basis. It may be that the best use of the data would be to test predictions from the model, for the strongest winds expected. If winds are indeed derived independently, they will provide strong constraints on the MTGCM simulations, and these winds obtained from MAVEN will help improve future versions of the MTGCM and other 3D thermosphere-ionosphere models.

8 ACC Experiment Summary

The MAVEN Accelerometer Experiment (ACC) will use atmospheric drag measurements, sensed by the MIMUs, and spacecraft position information to recover atmospheric density along the spacecraft path near the periapsis portions of its orbit, particularly during the five Deep-Dip campaigns. The approach—and for the most part, the team—is the same as that approach and those personnel that performed similar density derivations for the aerobraking phases of MGS, ODY and MRO. Combined with additional attitude control information, it may also be possible to derive cross-track winds during the Deep Dips and to extend the density derivation a scale height or two above the nominal periapsis altitude of 150 km during the regular (non-DD) science orbit phases.

The derived densities will be compared with nearly simultaneous MAVEN NGIMS (Mahaffy et al. 2014, this issue) measurements to provide a base from which the constituent distribution above the homopause can be studied using both measurements and atmospheric numerical models. Retrieved densities can also be compared to remotely sensed profiles of temperature/pressure made by the Imaging Ultraviolet Spectrograph (IUVS, McClintock et al. 2014, this issue). The remotely sensed IUVS measurements are not made simultaneously, nor are they collocated; however, they can be compared for regional and temporal trends, particularly during events like sudden warmings.

The ACC density and wind information will provide powerful constraints on atmospheric modeling and new knowledge on how lower atmosphere processes (e.g., dust storms, gravity waves) drive thermospheric activity and structure. By its judicious choice of the DD locations and times, MAVEN will significantly expand the present coverage of lower thermospheric structure in local time and season, while adding key samples of inter-annual and solar cycle variations. By enhancing our understanding (and modeling) of the current Martian atmosphere and its processes, the MAVEN ACC Experiment will aid the overall mission goal to better understand the long-term evolution of that atmosphere and the apparent loss of its volatiles early in its past.

References

D.T. Baird, R. Tolson, S.W. Bougher, B. Steers, Zonal wind calculations from Mars Global Surveyor Accelerometer and rate data. J. Spacecr. Rockets **44**, 1180–1187 (2007)

S.W. Bougher, Final report: JPL/CDP MAVEN project: coupled MGCM-MTGCM Mars thermosphere simulations and resulting data products in support of the MAVEN Mission. August 16 (2012)

S.W. Bougher, J.M. Bell, J.R. Murphy et al., Polar warming in the Mars thermosphere: seasonal variations owing to changing insolation and dust distributions. Geophys. Res. Lett. **33**, L02203 (2006). doi:10.1029/2005GL024059

S.W. Bougher, P.-L. Blelly, M. Combi et al., Neutral upper atmosphere and ionosphere modeling. Space Sci. Rev. **139**, 107–141 (2008). doi:10.1007/s11214-008-9401-9

D. Fritts, L. Wang, R. Tolson, Mean and gravity wave structures and variability in the Mars upper atmosphere inferred from Mars Global Surveyor and Mars Odyssey aerobraking densities. J. Geophys. Res. (2006). doi:10.1029/2006JA011897

J. Forbes, A. Bridger, S. Bougher, M.Hagan.J. Hollingsworth, G. Keating, J. Murphy, Nonmigrating tides in the thermosphere of Mars. J. Geophys. Res. (2002). doi:10.1029/2001JE001582

G.M. Keating, S.W. Bougher, R.W. Zurek et al., The structure of the upper atmosphere of Mars: in-situ accelerometer measurements from the Mars Global Surveyor. Science **279**, 1672–1676 (1998)

G.M. Keating, M. Theriot, R. Tolson et al., Brief review on the results obtained with the MGS and Mars Odyssey 2001 accelerometer experiments, in *Mars Atmosphere: Modeling and Observations Workshop, Granada, Spain* (2003)

B. Jakosky et al., The Mars Atmosphere and Volatile Evolution (MAVEN) Mission (2014, this issue)

P. Mahaffy et al., The neutral gas and ion mass spectrometer on the MAVEN Mission (2014, this issue)

W. McClintock et al., The imaging ultraviolet spectrograph for the MAVEN Mission (2014, this issue)

M. Smith, Interannual variability in TES atmospheric observations of Mars during 1999–2003. Icarus **167**, 148–165 (2004)

R. Tolson, G. Keating, R. Zurek, S. Bougher, C. Justus, S. Fritts, Application of accelerometer data to atmospheric modeling during Mars aerobraking operations. J. Spacecr. Rockets (2007). doi:10.2514/1.28472

R. Tolson, E. Bemis, S. Hough, K. Zaleski, G. Keating, J. Shidner, S. Brown, A. Brickler, M. Scher, P. Thomas, Atmospheric modeling using accelerometer data during Mars Reconnaissance Orbiter aerobraking operations. J. Spacecr. Rockets (2008). doi:10.2514/1.34301